Space charge effects in fourth-generation light sources: The PETRA IV and SOLEIL II cases

S. A. Antipov[1], V. Gubaidulin[2], I. Agapov[1], E. C. Cortés García[1], and A. Gamelin[2]

[1]*Deutsches Elektronen-Synchrotron DESY, Notkestr. 85, 22607, Hamburg, Germany*
[2]*Synchrotron SOLEIL, Saint-Aubin, 91190, France*

It is a truth universally acknowledged that space-charge effects in ultrarelativistic electron storage rings are irrelevant due to the steep inverse dependence of their strength on the Lorentz factor. Yet, with the push toward the diffraction limit, the state-of-the-art light sources are approaching the point where their emittance becomes so small that the space-charge force can no longer be ignored. In this paper, we demonstrate how space-charge effects influence the injection dynamics, dynamical aperture, and collective beam stability using the example of fourth-generation light sources PETRA IV and SOLEIL II.

I. INTRODUCTION

Accelerator lattices are typically designed with the aim of optimizing single-particle dynamics. However, when a charged particle orbits the accelerator, it sees the neighboring particles and interacts with them—a phenomenon known as the space-charge (SC) effect. This Coulomb interaction, nonlinear in nature, may lead to many unwanted consequences.

The nonlinear space-charge force alters single-particle dynamics in the ring, shifting the frequencies of transverse oscillations around the reference orbit (i.e., the incoherent tunes). It may lead to resonance excitation, emittance growth, halo formation, and losses [1–3]. Space charge also affects the collective dynamics in many ways. It has an effect on the frequencies of head-tail modes and can suppress transverse mode coupling instability [4]. At the same time, since it shifts the incoherent tunes, it also has an impact on Landau damping and suppression of head-tail instabilities [5–9]. Lastly, sufficiently strong SC can give rise to convective instabilities within high-intensity bunches [10].

The SC effects are the most prominent in the frontier high-intensity hadron machines, e.g., SPS (CERN), SIS100 (FAIR/GSI), and their injectors. Lepton rings, on the other hand, benefit from the much smaller mass of the particles as the SC interaction decreases with the Lorentz factor, which is typically orders of magnitude larger than in hadron rings. Yet, it has been noted that SC effects might be important in

the damping rings of a linear lepton collider where a combination of relatively low beam energy and small emittance makes SC interaction significant. SC has been found problematic, affecting coupling and low-order resonances in both ILC [11,12] and CLIC [13,14] designs.

Contemporary synchrotron light sources are few-hundred-meter- to kilometer-long electron storage rings, operating at energies around a few GeV. By design, they feature relatively large circumferences, necessary for achieving the smallest beam emittance and, thus, the largest photon brilliance. With the latest advances in multibend achromat focusing optics [15,16], the state-of-the-art fourth-generation light sources reach geometric emittances in the 10–100 pm range. At this level, the particle density within the bunch becomes so large that the SC effects might
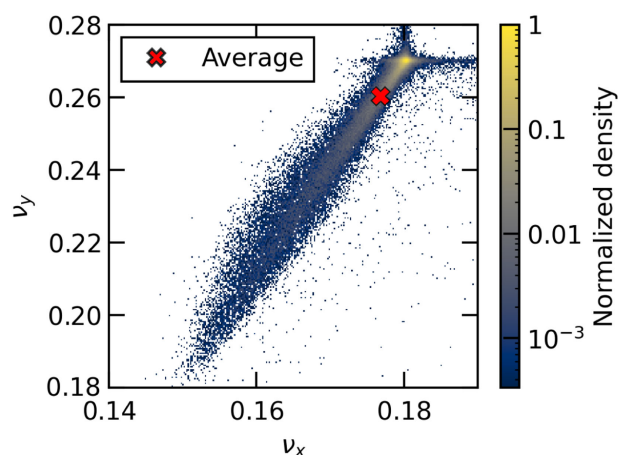

FIG. 1. Exemplary tune footprint with space charge of a 10 nC bunch in PETRA IV. Incoherent particle tunes spread far away from the nominal working point of (0.18, 0.27). Numerical simulation in Xsuite [18].

become important (Fig. 1). Nagaoka and Bane [17] predicted that the incoherent optics distortion produced by SC may have negative effects on machine performance, such as emittance increase, reduction of injection efficiency, and beam lifetime. Nevertheless, the topic of SC is frequently overlooked at the design stage of future light sources.

In this paper, we demonstrate that SC does indeed become significant for fourth-generation synchrotron light sources, both for single-particle and for collective dynamics. It can have an effect on various aspects of machine performance, from beam emittance to the intensity limit. We analyze its impact in detail on the examples of two fourth-generation light sources that cover the energy range of most future machines: a high-energy 6 GeV PETRA IV light source and a medium-energy 2.75 GeV SOLEIL II.

II. SPACE-CHARGE EFFECTS

Let us begin by introducing our two study cases. Both machines feature multibend achromat lattices [15,16] with tight focusing and beam sizes reaching as low as $\sigma \lesssim 10 \ \mu\text{m}$. The 6 GeV PETRA IV machine utilizes a hybrid H6BA lattice [19] with a large dynamic aperture and beam lifetime. It will be equipped with fast kickers for off-axis top-up injection. SOLEIL II is a more compact machine operating at a 2.75 GeV energy, with its higher order achromat lattice combining 4BA and 7BA cells [20,21]. It is designed to operate with a multipole injection kicker (MIK) for transparent injection [22]. Both machines have a double rf system comprising the main rf and a higher harmonic rf to stretch the bunches and increase the beam lifetime. PETRA IV will utilize active normal conducting 500 MHz main and 1.5 GHz third harmonic cavities, while SOLEIL II will use 352.20 MHz main cavities and 1.4 GHz passive normal conducting fourth harmonic cavities. The machines envisage delivering to users a high-beam current, low-charge brightness mode, and a high-charge timing

mode with a smaller number of bunches. Table I lists the key parameters of both machines.

A. Space-charge tune spread

Consider a beam of short relativistic electron bunches (charge e, mass m_e) orbiting the storage ring of a light source. The Coulomb interaction between the particles will change their natural frequencies of oscillation around the reference orbit, causing a so-called space-charge tune shift. In the linear model, the maximal tune shift of a Gaussian bunch can be estimated as

$$\Delta\nu_{x,y}^{\text{SC}} = -\frac{Nr_eC}{(2\pi)^{3/2}\gamma^3\sigma_z}\left\langle\frac{\beta_{x,y}}{\sigma_{x,y}(\sigma_x+\sigma_y)}\right\rangle, \quad (1)$$

where N is the number of particles per bunch, $\sigma_{x,y,z}$ are the rms horizontal, vertical, and longitudinal beam sizes, γ is the Lorentz factor, $\beta_{x,y}$ are the transverse Twiss optics functions, and $\langle\ldots\rangle$ denotes averaging over the ring circumference C. $r_e = e^2/m_ec^2 \approx 2.8 \times 10^{-13}$ cm (in cgs units) stands for the classical electron radius and c is the speed of light. In a typical scenario of a machine operating with flat beams, $\sigma_y \ll \sigma_x$, the largest tune shift occurs in the vertical, y-plane.

While the $1/\gamma^3$ factor can be as small as 10^{-12} in a GeV range light source, it is compensated by the second term in Eq. (1). The small beam size may result in an SC tune shift of the order of or larger than the synchrotron tune. For example, in PETRA IV, if operated without the third harmonic cavities, the SC tune shifts reach a level of 10^{-2} for the low-charge brightness mode and nearly 0.1 for the high-charge timing mode (Table II). This is significant and might affect the single-particle nonlinear dynamics in the ring. A measure of SC impact on the collective instabilities is the SC parameter, i.e., the ratio of its tune shift to the synchrotron tune $|\Delta\nu_y^{\text{SC}}|/\nu_s$. At $|\Delta\nu_y^{\text{SC}}|/\nu_s \sim 5\text{--}20$, depending on the bunch charge, the SC is expected to play a role in the collective dynamics as well. With the bunch lengthening, third harmonic cavities, the SC tune shift decreases to $1 - 4 \times 10^{-2}$, still a significant figure.

TABLE I. PETRA IV and SOLEIL II machine parameters and their main baseline operation modes: Brightness and timing (in parenthesis).

Parameter	Symbol	PETRA IV	SOLEIL II
Energy (GeV)	E	6.0	2.75
Circumference (m)	C	2304	354
Momentum compaction	α_C	3.3×10^{-5}	1.07×10^{-4}
Betatron tunes	$\nu_{x,y}$	135.18, 86.27	54.2, 18.3
Operational chromaticities	$\xi_{x,y}$	6, 6	1.6, 1.6
Main rf frequency (MHz)	f_{rf}	500.0	352.20
Synchrotron tune	ν_s[a]	0.005	0.002
Bunch charge (nC)	Q_b	1 (8)	1.4 (7.4)
Rms bunch length (ps)	σ_t	40 (65)	42 (50)
Emittance (pm rad)	ϵ_0	20	83
SR damping times (ms)	$\tau_{x,y,s}$	18, 22, 13	8, 14, 12

[a]Without the harmonic rf system.

TABLE II. Estimated SC tune shifts in PETRA IV (PIV) and SOLEIL II (SII).

		w/harm cav		w/o harm cav	
	Q_b (nC)	$\Delta\nu_x$	$\Delta\nu_x$	$\Delta\nu_x$	$\Delta\nu_x$
PIV	1	-2.8×10^{-3}	-1.0×10^{-2}	-7.6×10^{-3}	-2.7×10^{-2}
	8	-1.2×10^{-2}	-4.1×10^{-2}	-2.2×10^{-2}	-7.7×10^{-2}
SII	1.4	-3.1×10^{-3}	-6.2×10^{-3}	-8.8×10^{-3}	-1.8×10^{-2}
	7.4	-1.4×10^{-2}	-2.9×10^{-2}	-2.7×10^{-2}	-5.4×10^{-2}

Note that the case of PETRA IV is somewhat special as, inheriting its ring tunnel from the high-energy physics program, PETRA features a relatively large circumference for its energy, resulting in a large SC tune shift. This would also be the case for other ex-collider machines, such as a potential ring in the PEP tunnel at Stanford [23,24]. "More conventional" light sources normally have a circumference between 300 and 500 m for ~3 GeV machines and about 1 km for 6 GeV machines. For instance, a fourth-generation 2.75 GeV light source SOLEIL II will have a 354 m circumference (Table I). Its bright beams will have $|\Delta\nu_y^{\mathrm{SC}}|/\nu_s \sim 2{-}25$ without a harmonic cavity.

In the present-day third-generation light sources, the SC tune shifts are significantly smaller thanks to the much greater transverse emittance. For example, PETRA III has $\epsilon_x \approx 1$ nm with the highest bunch charge of 19 nC in a 40-bunch timing mode [25]. Under these conditions, the SC tune shift is $\sim -6 \times 10^{-3}$, while $\nu_s = 0.049$ and the SC parameter $|\Delta\nu_y^{\mathrm{SC}}|/\nu_s \approx 0.1$, a rather small quantity to have any meaningful effect on the beam. In SOLEIL [26], $\epsilon_x \approx 3.9$ nm and $\Delta\nu_y^{\mathrm{SC}} \sim -1.4 \times 10^{-3}$ for a nominal charge of 1.4 nC and $\Delta\nu_y^{\mathrm{SC}} \sim -5 \times 10^{-3}$ for the highest possible charge of ~25 nC, while $\nu_s = 4.8 \times 10^{-3}$. The SC parameter in the case of SOLEIL is $|\Delta\nu_y^{\mathrm{SC}}|/\nu_s \lesssim 0.1{-}1$. In this case, there should not be a significant effect on the beam dynamics.

B. Longitudinal space charge

It is worth mentioning that while the transverse SC might be significant thanks to the small beam size, the same is not the case for the longitudinal SC. Indeed, the synchrotron SC tune shift scales with $\ln(b/\sigma_y)$, where b is the radius of the vacuum chamber [27]. This logarithm does not exceed ~10, and the tune shift is

$$\Delta\nu_s^{\mathrm{SC}} \sim -\frac{N\alpha_C r_e C^2}{8\pi^2\gamma^3\nu_s\sigma_z^3}.\tag{2}$$

For the beam parameters in Table I, $\Delta\nu_s^{\mathrm{SC}} \lesssim 10^{-7}$, which is a negligibly small quantity.

C. Space-charge-driven resonances

Space-charge force, nonlinear in nature, produces a rich variety of resonance conditions in a machine [28]. In particular, because the SC force depends on the longitudinal position of a particle within the bunch, a particle performing synchrotron oscillations will, therefore, experience a tune modulation with twice the synchrotron tune ν_s. For a flat beam, where the vertical SC force dominates, this leads to a resonance condition [11]

$$n\nu_x + m(\nu_y \pm 2\nu_s) = l,\tag{3}$$

where $l, m, n \in \mathbb{Z}$. In principle, the presence of SC-specific resonance lines might affect the boundary of the chaotic region in the phase space, limiting the dynamic aperture of

the machine and leading to injection losses. However, the SC effect is only experienced by particles that are in the core of the stored bunch. Particles still exerting ample betatron oscillations (e.g., after a top-up injection) will not be affected by it.

D. Mitigation of transverse mode coupling instability

Another important effect of SC is its shift of frequencies of coherent head-tail modes, which manifests itself in the mitigation of transverse mode coupling instability (TMCI) of modes 0 and -1 [4]. The TMCI limits the bunch charge at chromaticity 0 (here, and later, we denote *unnormalized* chromaticity as ξ). It is characterized by a fast rise time of the order of a synchrotron period, which is typically much faster than the synchrotron radiation (SR) damping time. A normal resistive feedback is also inefficient at suppressing the instability and, in fact, may have a destabilizing effect [29]. While TMCI can be mitigated by a simple increase in ξ, there may be other considerations in favor of working at a low chromaticity, such as a smaller sextupole strength, which might result in a larger DA, better injection efficiency, and lower power consumption.[1] The TMCI threshold for a zero chromaticity lattice is approximately [31]

$$Q_{\mathrm{th}} = 8\pi^{3/2}\frac{E}{e}\frac{\nu_s\sigma_z}{C}\min\left(\frac{\nu_{x,y}}{Z_{x,y}}\right),\tag{4}$$

where ν_s is the synchrotron tune, $Z_{x,y}$ is the effective transverse impedance, and E is the beam energy. Typically, in a light source, it is the y-plane that poses the limitation due to the larger beam coupling impedance because of the narrow undulator chambers. The formula is valid for a single-harmonic rf system, assuming that the bunch lengthening from longitudinal impedance is small.

E. Landau damping by space charge

The large nonlinear betatron tune spread generated by SC gives rise to Landau damping of collective head-tail modes in the electron bunches. From the results obtained for hadron synchrotrons analytically [7–9] and in simulations [5,32], one might expect a strong suppression of head-tail instabilities by SC in the region $|\Delta\nu_y^{\mathrm{SC}}|/\nu_s \in [2, 20]$.

A few notable differences exist between the high-intensity hadron machines and low-emittance electron synchrotrons, though. First, the low-emittance ring design dictates strong focusing, resulting in smaller vacuum

---

[1]While in simulations the DA of PETRA IV does not change significantly with chromaticity, this might not be the case in a real machine due to magnet errors and imperfections. Experience on a fourth-generation ESRF EBS light source, which utilizes a similar HMBA lattice, suggests the presence of an optimal sextupole setting that maximizes beam lifetime [30].

chamber dimensions and stronger impedance effects. This leads to impedance-induced coherent tune shifts of the order of ν_s. Thus, individual head-tail modes cannot be treated independently. Second, the transverse wakefield force cannot be assumed to be much smaller than the space-charge force, as is the case in [5,7–9,32]. Consequently, the impedance-induced tune shifts cannot be assumed to be much smaller than those created by SC. Finally, the electron storage rings are more susceptible to the high-frequency impedance components due to their shorter bunch length: 10–100 ps vs 1–1000 ns in hadron machines.

III. PETRA IV CASE

As the first example of SC affecting the beam dynamics, let us consider the case of the 6 GeV PETRA IV machine in more detail. To study the effect of SC on PETRA IV, simulation campaigns were carried out with ELEGANT [33]. We investigated the impact on the dynamic aperture, the dynamics of the off-axis top-up injection, and the single-bunch charge accumulation limit.

A. Simulation setup

Our simulation setup included 6D element-by-element tracking, effects of synchrotron radiation, quantum excitation, longitudinal and transverse dipolar, and quadrupolar impedance. The impedance model accounts for all major sources of wakefields in the ring: the vacuum chambers, rf cavities, injection and feedback kickers, BPMs, current monitors, tapers, bellows, and radiation absorbers. The resistive wall contributions of components were computed with IW2D, including the planned NEG coating of vacuum chambers (resistivity of 2 μΩm, according to rf measurements of coated tube samples). The geometric part of the impedance has been computed using CST Particle Studio and GDFIDL codes.

Misalignment and gradient field errors were introduced to generate an rms β beat of ∼3%. The coupled-bunch dynamics was outside of the scope of this first SC study due to the computational complexity of the problem (1920 bunches in the brightness mode). The intrabeam scattering (IBS) was taken into account indirectly by initializing the beam with charge-dependent distribution parameters, obtained from a separate study of IBS. This approach is justified when focusing on the onset of collective instabilities and simulating the timescales of about an SR damping time. At these timescales, the distribution should not have changed significantly due to the absence of IBS from our tracking, thanks to the high beam energy, which reduced the IBS growth rates.[2] The direct SC element in ELEGANT follows a quasifrozen model

and only includes transversal nonlinear effects. The model utilizes the Basetti-Erskine approximation [35] to compute the electric field of an ultrarelativistic Gaussian bunch and updates the kick strength according to the local beam parameters [12]. SC kicks were added at every quadrupole to simulate the effect at each turn, while also sampling the evolution of the beam size around the ring. This is a sufficient number of kicks in order to achieve numerical convergence in terms of equilibrium beam emittances (Appendix A).

In addition, Xsuite [18] was used to run tracking simulations for an independent benchmark. The tracking configuration retains all of the effects from ELEGANT, except for misalignment and gradient field errors. Three types of SC kicks in Xsuite are available: particle-in-cell (PIC), frozen, and quasifrozen. SC kicks with the PIC model were inserted into the lattice at equal intervals to support the findings from the ELEGANT. Benchmarks are included in Appendix B. If not otherwise stated, SC kicks in Xsuite were introduced with the quasifrozen model.

B. Dynamics of top-up injection

In the case of PETRA IV, pursuing an off-axis injection scheme, the dynamics is, in first instance, dictated by the strong amplitude detuning imposed by the HMBA lattice. Particles in the injected bunch possess a distinct tune value, far from the nominal. While the tune depression described by Eq. (1) is incoherent, it effectively spreads the tune distribution and shifts its average. This implies that under strong SC influence, the injected bunch can find itself at a different working point. To account for this effect, one could naively shift the nominal working point. However, while a tune correction (e.g., with a tune feedback system) could restore the average tunes of the machine, significantly detuned particles will still remain. Moreover, the same correction would affect the tunes of the injected bunch during the off-axis injection. The tune of the injected bunch is sketched in Fig. 2. SC affects the trajectory of the injected bunch on the tune diagram as it damps down to the reference orbit. When applying tune correction, the injected bunch would trace a different path depending on the charge of the stored bunch. Also, considering the stop band width excited by misalignments and gradient field errors, displacing the working point might reduce the injection efficiency. This can be seen in Fig. 2(b), where a tune correction intended to bring the tunes of the stored bunch back to its nominal working point displaces the tunes of the injected bunch toward a half-integer resonance.[3] This way the presence of charge-dependent tune shift may pose constraints on the tune correction and injection amplitude.

---

[2]The overall impact of IBS on the equilibrium horizontal emittance is below 5 pm in the brightness mode with harmonic cavities [34].

[3]In reality, the width of the resonance stop band might differ depending on the actual errors and misalignments of a real machine.
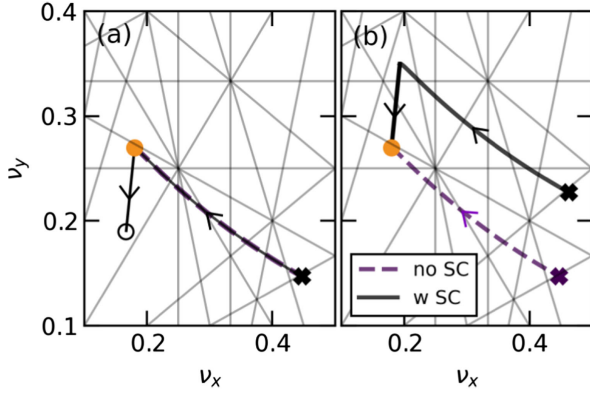
FIG. 2. Evolution of particle tune during the off-axis injection process with and without taking the SC force into account. (a) Nominal tunes; the SC shifts the average tune of the stored bunch (black circle) from its set point (orange dot). (b) Assuming a tune correction applied to bring the average tune with SC to the set point value (orange dot); the tune correction affects the tune of the bunch injected off axis (cross). The curves represent the excursion of off-axis injection of a flat beam, the crosses represent the extension of a particle at 3 rms from the injected bunch centroid. Bunch charge 20 nC, bunch lengthening by longitudinal wakefields, and third harmonic rf included.

C. Dynamic aperture

Our studies found no harmful effect of the SC-driven resonances on the nominal PETRA IV working point. At the same time, a significant effect will be present if one decides to operate at a high coupling. Figure 3 shows an exemplary tune footprint for a 10 nC bunch and an emittance coupling ratio close to 1. One can clearly observe the excitation of the SC-driven resonance line, in line with Eq. (3). This may result in a change of the emittance ratio, forcing the beam to become more round as it approaches
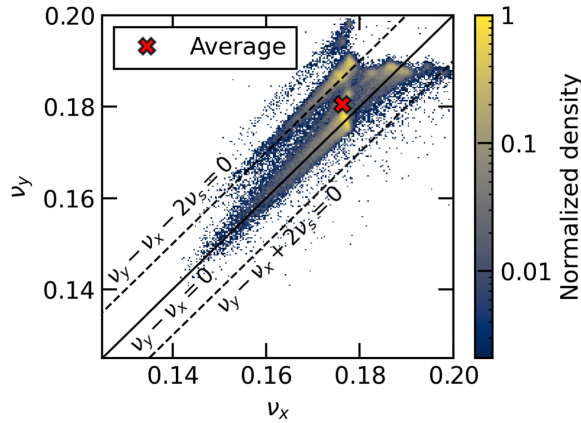

FIG. 3. SC tune footprint of a high-charge bunch close to the coupling resonance. Bunch charge 10 nC, tune set point: 0.18, 0.185, only the main rf system. Simulation in Xsuite [18]. Particles group themselves around the coupling (solid line) and the SC-driven (dashed lines) resonance. The average incoherent tune is denoted with a cross.

the coupling resonance $\nu_x - \nu_y \rightarrow -0$ (Fig. 4). When $\nu_x > \nu_y$, the negative SC tune shift, being larger in the vertical plane, drives the beam away from the coupling resonance, thus making the beam less round than it otherwise would have been. As this change of emittance ratio is charge-dependent, it might complicate the operation of the machine at full coupling.

D. Collective stability

Synchrotron light sources rely on a combination of chromaticity, synchrotron radiation damping, and active feedback to ensure single- and coupled-bunch stability. Landau damping is normally negligible due to the small beam size and therefore small amplitude-dependent betatron tune spread within the bunches. Space charge can create a significant amount of betatron tune spread, thus adding Landau damping as an additional tool at the disposal of accelerator physicists. In the following section, we consider the effect of SC on transverse single- and coupled-bunch dynamics.

1. Stabilization at chromaticity 0

In the absence of SC the TMCI threshold at $\xi = 0$ for the PETRA IV light source ($Z_y \approx 1.3$ MΩ/m) is 0.5 nC without lengthening cavities, according to Eq. (4). Applying Eq. (4) to the case with the third harmonic rf ($\langle \nu_s \rangle = 1.7 \times 10^{-3}$), we obtain $Q_{th} = 0.3$ nC. These limits are in good quantitative agreement with our tracking in ELEGANT [Figs. 5(a) and 5(b)], in which we tracked the beam for 4096 turns, or about 1.5 synchrotron radiation damping times, taking into account bunch lengthening by self-induced wakefields.

Including the SC in our tracking simulation, we observe that it effectively mitigates the TMCI. Without the third harmonic cavity, neglecting the SC yields a single-bunch charge threshold of about 0.7 nC [Fig. 5(a)] with the bunch becoming unstable in the vertical plane and its beam size
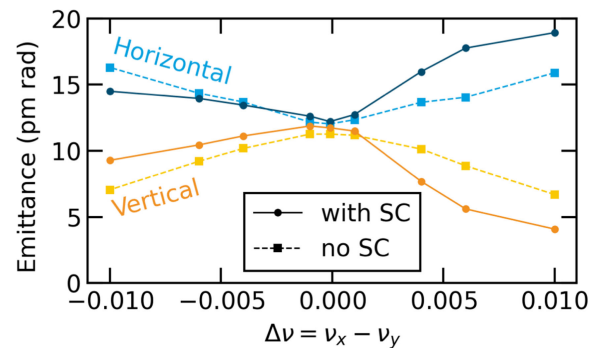

FIG. 4. Transverse emittances as functions of tune separation. Tune depression caused by space charge affects emittance ratios. Lighter dashed lines depict the situation without SC force; darker solid ones—with SC. Bunch charge 10 nC only main rf system, no wakefields, $\xi = 0$.
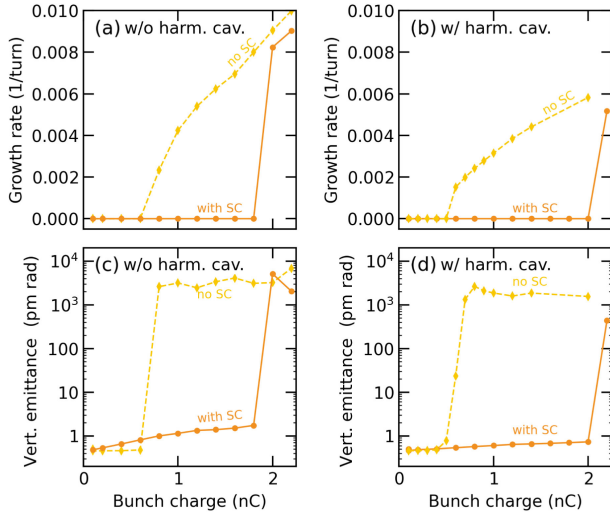
FIG. 5.   Space charge mitigates TMCI instability at chromaticity 0. The exponential growth rates of the c. m. motion in the vertical plane with and without the harmonic rf (a), (b) and the final vertical beam emittance after 4096 revolutions, or 20 synchrotron periods, (c), (d) as a function of bunch charge at $\xi = 0$. All results were obtained using element-by-element tracking in ELEGANT with a realistic 3% beta beating.
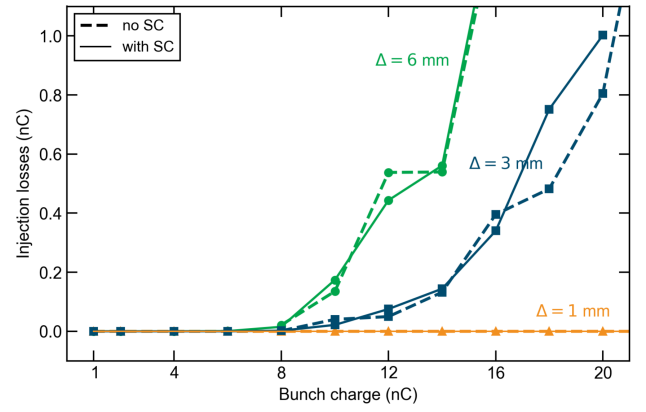

FIG. 6.   When the stored bunch is significantly displaced from the reference orbit at injection (e.g., during the aperture sharing), the SC has no effect on the resulting losses. Three aperture sharing amplitudes Δ considered from 1 to 6 mm. Element-by-element tracking in ELEGANT with a realistic aperture model and 3% beta beating.

rapidly increasing.[4] The final beam emittance is shown in Fig. 5(c): above the instability threshold, the beam emittance is significantly degraded. The SC leads to two effects: first, the instability is stabilized, and the intensity threshold increases to about 1.9 nC, nearly 3 times higher [Fig. 5(a)]; second, below the new threshold the vertical emittance steadily increases with the bunch charge due to the additional coupling produced by SC [Fig. 5(c)].

With the bunch lengthening third harmonic rf in place, one observes a similar picture. Without the SC force, the bunch becomes vertically unstable at about 0.5 nC, but when we include the SC, it remains stable well above this threshold [Fig. 5(b)]. In this case, we do not observe such a significant increase of the vertical emittance with the bunch charge as without the third harmonic rf [Fig. 5(d)], likely due to the large bunch length and, hence, smaller charge density.

2. Single-bunch accumulation limit

Accumulation of bunch charge during off-axis top-up injection requires that the injection losses, both in the stored and in the injected beams, be relatively small compared to the injected charge. As soon as the injected losses approach the injected charge, further accumulation is not possible.

At PETRA IV, significant injection losses happen in the stored bunch when employing aperture sharing, i.e., the injection bump is intentionally not closed to provide additional room for the injected beam. After the injection kick, the stored beam rapidly decoheres in a few turns and its density drastically decreases. Because of this SC cannot have any significant effect on the injection dynamics when employing aperture sharing. Element-by-element tracking in ELEGANT confirms this hypothesis: no significant difference in the amount of injection losses has been observed
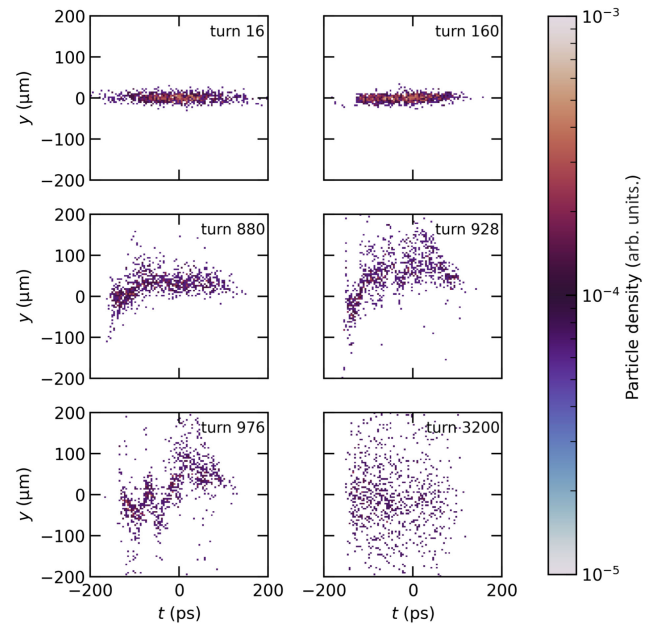

FIG. 7.   Head-tail instability developing in the vertical plane after injection at turn 0. Bunch charge 14 nC, chromaticity 5, no SC. Color denotes the beam density on a logarithmic scale.

---

[4]The rapid growth rates, typical to TMCI, were found in tracking by observing the amplitude of the c. m. motion with a 200-turn moving window and fitting it with an exponential process.
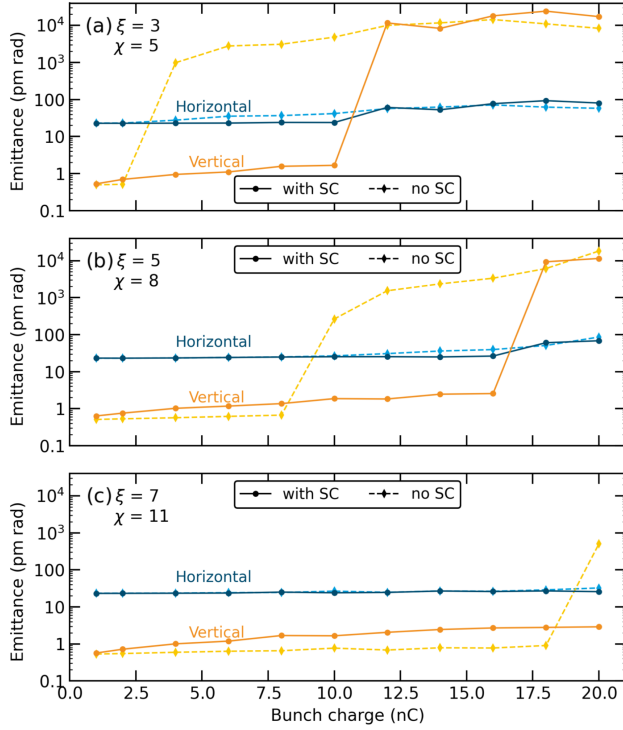
FIG. 8. As the bunch charge increases the vertical emittance is blown up by the head-tail instability. Space charge helps stabilize the beam, increasing the single-bunch current limit. Chromaticity 3 (top), 5 (middle), and 7 (bottom) with third harmonic rf and 3% beta beating.
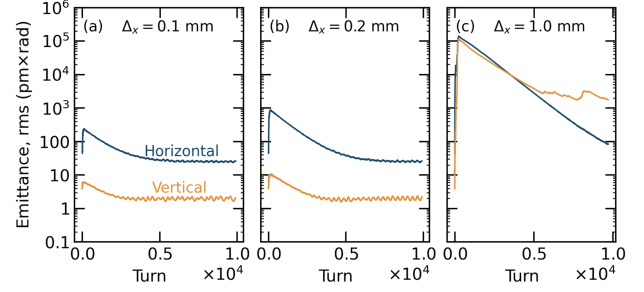

FIG. 9. Evolution of the rms emittance of the stored bunch after a small parasitic kick during the top-up injection (a), (b). The injection kick of a large enough amplitude might destabilize the bunch that has been kept stable by SC, blowing up its emittance (c). Bunch charge 12 nC, chromaticity 5, 3% rms beta beating.

when tracking the beam for 4096 turns after the injection (Fig. 6) at $\xi = 5$, which corresponds to an rms head-tail phase advance $\chi = \xi \times 2\pi\sigma_z / C\alpha_C = 8$.

At the same time, even if the losses are not considerable, the beam quality might be compromised by a head-tail instability triggered by the injection event (Fig. 7). The instability rapidly increases the beam size to about 100 times the initial one. Further blowup and particle losses do not happen, which can be attributed to the nonlinear amplitude detuning providing sufficient Landau damping to suppress the instability growth. Such a blown-up beam is doubtfully useful for the photon science because of its low brightness. The SC provides an additional stabilization mechanism and helps mitigate the head-tail instability (Fig. 8). This allows accumulating a greater bunch charge without compromising the beam quality.

Thus, in the presence of space charge our dynamical system may have two distinct equilibrium states: the low-emittance state, where it is stabilized by the nonlinearity of the space charge, and the high-emittance state, where it is stabilized by the nonlinear amplitude detuning. The former state is unstable in nature, so a small increase in beam emittance can lower the stabilizing space-charge force, reducing the strength of Landau damping and making the

beam unstable, further increasing the emittance. The latter is a stable equilibrium state as a small increase of beam emittance would only further increase the nonlinear tune spread, enhancing the Landau damping.

To illustrate that the high-bunch-charge state stabilized by SC is an unstable equilibrium, let us consider small injection perturbations of the stored bunch that might result from an imperfect closure of the injection bump. At PETRA IV, the injection bump amplitude is 10 mm, and it is estimated that the field quality in the kickers as well as the pulse shape stability in the power supplies guarantee a relative stability of the injection kick at the 10^{-3} level [36]. That is, we do not expect injection bump nonclosures far beyond 100 μm in operation. Yet, for the sake of making an argument, we will consider larger values here. Let us consider a bunch that should be unstable without space charge but is stabilized by it, e.g., 12 nC at $\xi = 5$ [Fig. 8(b)]. Assume there is an injection bump nonclosure in the x-plane. Due to nonzero coupling between the transverse planes, the bunch will execute small oscillations in both planes after injection, resulting in an increase of its projected emittances. For small bump amplitudes, ca. 100–200 μm, the bunch remains stable and the synchrotron radiation damps the emittances down to their unperturbed equilibrium values [Figs. 9(a) and 9(b)]. When the nonclosure is large, i.e. 1 mm [Fig. 9(c)], the dynamics is altered. The SC no longer stabilizes the bunch and the vertical emittance settles at the value it would have if there were no SC, about 10^4 pm rad, 3 orders of magnitude larger than that of an unperturbed bunch.

In order to prevent the degradation of beam quality, one may consider increasing the chromaticity, which keeps the bunch stable without the SC [Fig. 8(c)]. However, for the sake of a larger DA and a longer beam lifetime, it might be beneficial to operate at lower ξ. Then one may take advantage of the stabilization offered by the SC by keeping the chromaticity at an optimal, potentially lower setting during the fill and increasing it only temporarily during top-up injections.

IV. SOLEIL II CASE

Since SOLEIL II plans use MIK for injection [22], this avoids the need for aperture sharing, and therefore, no collective effects are expected at injection. Yet, the SC might still have an effect on the stored beam. The expected space-charge tune shifts in SOLEIL II are relatively large and are displayed in Table II.

A. Simulation setup

The primary tool for studying collective effects at SOLEIL is the particle tracking code MBTRACK2 [37,38]. The code allows us to simultaneously consider single- and coupled-bunch collective effects in transverse and longitudinal planes. A linearized Vlasov equation solver, DELPHI [39], is used additionally if required. Transverse space charge was recently implemented in MBTRACK2 using a Basetti-Erskine formula [35] with a so-called matched frozen space-charge model [40]. The longitudinal bunch profile is used to modulate the strength of the space-charge kick.

Simulations in this paper are based on the lattice parameters reported in [21]. Simulations in MBTRACK2 are dedicated to collective effects, so a few simplifications are made. All simulations include the following elements: a one-turn map for transverse motion, a detuning model of chromaticity, synchrotron radiation effects, transverse short and long-range wakefields, longitudinal short-range wakefield, rf cavities setup, and a lumped space-charge kick. We use the full impedance model of SOLEIL II with more than 50 distinct elements.[5] The geometric part of the impedance was computed with CST Particle Studio and ABCI. NEG-coated resistive wall and image charge contributions were obtained with IW2D. In all cases, for the first 25,000 turns, only longitudinal wakefield acts on the beam to reach an equilibrium bunch length. After which transverse wakes are turned on, and the beam is tracked for another 25,000–75,000 turns. A total of 1,000,000 macroparticles per bunch are used in all simulations. The bunch is partitioned into 100 longitudinal slices for wakefield and space-charge interactions.

Results without space charge, the corresponding simulation setup, the impedance model of SOLEIL II, the current harmonic cavity configuration, and transverse feedback requirements were discussed in detail in [41]. The effect of IBS is only included when specified. IBS is modeled in tracking using a simple kick model [42] based on an analytical calculation of the IBS growth rate at every turn. We have employed the completely integrated Piwinski

---

[5]The current impedance model of SOLEIL II does not yet include quadrupolar wakefields. As the vacuum chamber of SOLEIL II is round, many of the impedance model components are axisymmetric, except for the in-vacuum IDs; it is expected that quadrupolar wakes are less important in SOLEIL II than they are in third-generation light sources.
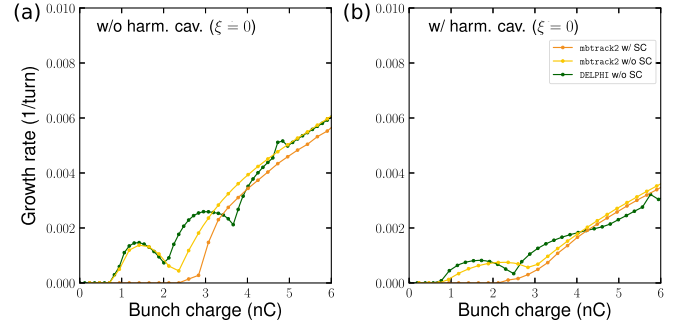

FIG. 10. Mitigation of TMCI by space charge for the case of SOLEIL II. The instability growth rates are plotted against the bunch current. (a) The case without a harmonic cavity; (b) the case with a harmonic cavity.

model [43] for growth rate calculation. This paper considers only vertical instabilities for SOLEIL II with closed gaps of insertion devices to obtain the strongest instabilities. The growth rates of all considered instabilities are found by fitting the beam c. m. offset with an exponential function.

B. Single-bunch instabilities

1. Transverse mode-coupling instability

Coupling of the azimuthal modes -1 and 0 causes a transverse mode coupling instability. Figure 10 compares the growth rates of TMCI with and without space charge for two cases. One case [Fig. 10(a)] shows a configuration without a harmonic cavity, and another [Fig. 10(b)] shows one with one included. In both cases, space charge leads to a more than twofold increase of the TMCI threshold current. It is well known [4] that space charge can delay or even prevent the coupling of azimuthal modes -1 and 0.

Figure 11 demonstrates the coherent frequencies of bunch oscillations as a function of bunch charge. In the case without space charge [Fig. 11(a)], modes -1, and 0 couple at ~ 0.9 nC and determine the TMCI threshold.
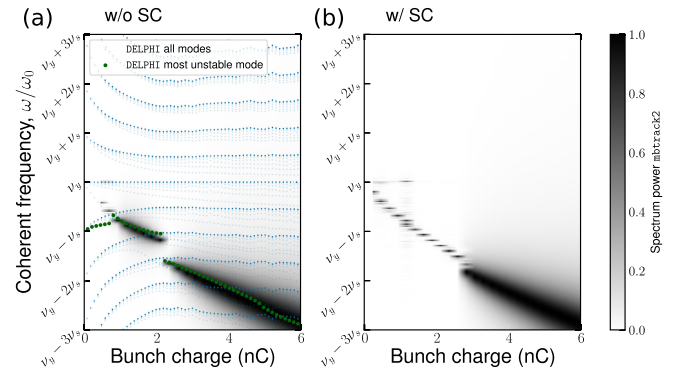

FIG. 11. Coherent frequencies of oscillations before and after the TMCI threshold w/o harmonic cavity. (a) Case w/o SC, compared to analytical solutions of DELPHI. (b) Case w/ SC.
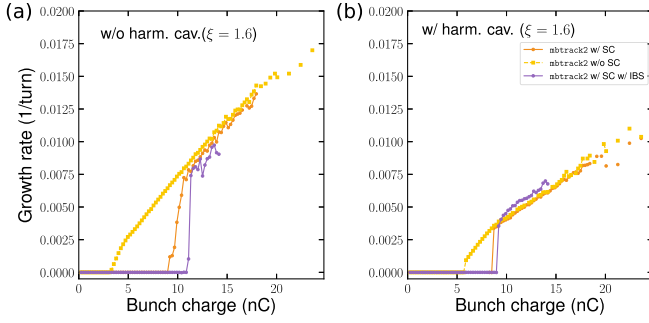
FIG. 12. Suppression of head-tail instability for the case of SOLEIL II. The instability growth rate is plotted against the bunch current. (a) The case without a harmonic cavity; (b) the case with a harmonic cavity.

At an even higher charge ~ 2 nC modes -3 and -2 couple and drive the instability.

With space charge [Fig. 11(b)], the TMCI threshold is now at ~ 2 nC. After the threshold, the bunch oscillates at similar frequencies as in the case without space charge for the same bunch charge. This can be interpreted as follows. Space charge prevented coupling of modes -1 and 0. However, the modes -3 and -2 still couple at a similar bunch charge regardless of space charge.

2. Head-tail instability

Figure 12 compares growth rates of head-tail instability with and without space charge. Two cases are again considered at the $\xi = 1.6$ design chromaticity. One without including a harmonic cavity ($\chi = 1.1$ at $Q = 1.4$ nC) and the other with a harmonic cavity ($\chi = 3.3$ at $Q = 1.4$ nC). In both cases, space charge completely suppresses head-tail instability up to ~ 8 nC. The instabilities are suppressed by Landau damping due to the space charge of a bunched beam. This strong suppression of head-tail instability by space charge (for the intermediate space-charge parameter values $|\Delta\nu_y^{SC}|/\nu_s \in [2, 20]$) is qualitatively consistent with results obtained for hadron synchrotrons analytically [7–9] and in simulations [5,32].

Figure 12 also compares growth rates obtained with space charge for two scenarios: with and without including IBS in the simulation. For Fig. 12(a), there is a notable difference in obtained threshold (~ 8 nC without IBS and ~ 11 nC with IBS). This can be interpreted in the following manner. From hadron machine research, it is known that space charge provides Landau damping in bunches only for the intermediate space-charge parameter. In our case, we assume that the instability threshold is determined by the loss of Landau damping due to the high value of the space-charge parameter. IBS will increase the beam emittance, thus reducing space-charge tune shift and increasing the instability threshold. For Fig. 12(b), a similar but smaller increase in the threshold bunch charge is observed.
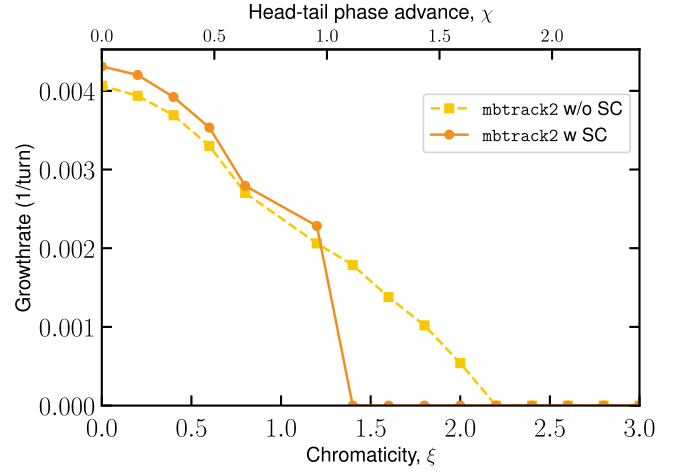

FIG. 13. Mitigation of TCBI in SOLEIL II by a combination of space charge and chromaticity w/o harmonic cavity.

This corresponds to the weaker IBS effect for bunches lengthened by a harmonic cavity.

C. Transverse coupled-bunch instability

Figure 13 shows the growth rates of transverse coupled-bunch instability (TCBI) for SOLEIL II brightness operation mode with 416 bunches at 500 mA for different settings of chromaticity ξ for the case without a harmonic cavity. It demonstrates that TCBI is suppressed for chromaticities $\xi > 1.5$ due to space charge. At these higher chromaticities, transverse coupled-bunch instability is already determined by both intrabunch and interbunch motions [44]. Space charge does not affect pure TCBI at $\xi = 0$ with $m = 0$ intrabunch mode, as seen from very close growth rates in Fig. 13. However, at higher chromaticities, this mode is known [45] to be overtaken by higher modes ($m \geq 1$) that can be affected by space charge.
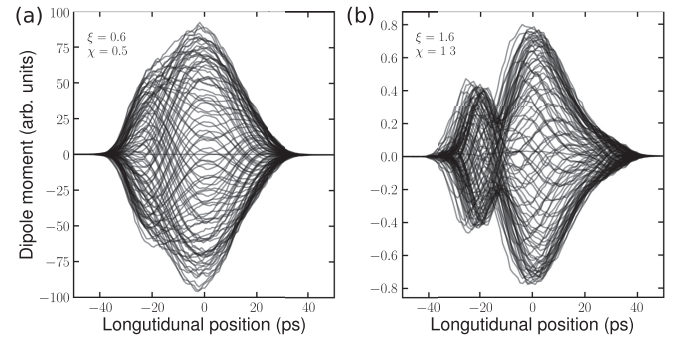

FIG. 14. Intrabunch motion (dipolar moment) of one of the bunches for (a) $\xi = 0.6$ and (b) $\xi = 1.6$ w/o SC. Obtained from MBTRACK2 simulations of Fig. 13 for 1.4 nC bunch charge.

Indeed, Fig. 14 demonstrates two different intrabunch modes $|m| = 0$ (at $\xi = 0.6$) and $|m| = 1$ (at $\xi = 1.6$) for the case without space charge. We considered the brightness mode of SOLEIL II with 416 equidistant bunches at 1.4 nC equivalent to 500 mA beam current. For the timing mode of SOLEIL II, the coupled-bunch instability is already suppressed by synchrotron radiation. As expected at low chromaticity (e.g., $\xi = 0.6$), intrabunch motion corresponds to $|m| = 0$ mode. At higher chromaticity (e.g., $\xi = 1.6$), it corresponds to $|m| = 1$ mode instead. At low chromaticities, the growth rates of the instability with and without space charge are very similar. When instability is dominated by $|m| = 1$ mode, space charge suppresses it. This demonstrates that space charge can affect coupled-bunch instabilities for sufficiently high chromaticities. Therefore, it can help to relax the requirements for a transverse feedback system that is usually employed to suppress this instability.

V. CONCLUSION

In this paper, we have studied the role of space charge in future fourth-generation light sources. Thanks to their small transverse beam size, these light sources attain significant space-charge tune shifts with the space-charge parameter approaching values as high as ~10 units. This results in a wide variety of new physics that is not typically observed in contemporary electron machines.

On the positive side, SC mitigates the mode coupling instability of modes 0 and 1 and increases the single-bunch current threshold at chromaticity 0, as seen in numerical simulations of PETRA IV and SOLEIL II machines. At higher positive chromaticities, SC increases the single-bunch intensity limits. It can also stabilize the coupled-bunch motion, lowering the required chromaticity setting, as observed in the 416-bunch mode of SOLEIL II. This additional instability mitigation by space charge can reduce the requirements for a transverse feedback system. The beam stabilization with space charge can be affected by IBS, especially when operating without a harmonic rf system. Depending on beam parameters, the IBS effect might be beneficial for further increasing the stability threshold, as observed in SOLEIL II. A harmonic rf system, normally designed to reduce the effect of IBS as much as possible, greatly diminishes its impact on beam instabilities.

On the other hand, SC also generates transverse coupling leading to rounder beams at high intensities. As we observe in our PETRA IV simulations, the large SC tune shift might interfere with the dynamics of the top-up injection. SC can also excite particular resonance lines, increasing the transverse emittance. This might compromise the beam quality, e.g., when operating close to a coupling resonance. Finally, the large SC tune shift might complicate the modes of machine operation with

high single-bunch charges when not employing bunch-lengthening cavities as seen with the timing mode of PETRA IV.

The fact that the stabilizing effect of SC is observed both in medium- and high-energy light sources and in different simulation setups, as well as expected from the theory, dictates that SC has to be taken into account if one wishes to accurately describe beam dynamics in future low emittance generation light sources.

APPENDIX A: CONVERGENCE TEST

The minimum number of SC kicks required for convergence was assessed by introducing an increasing amount of SC kicks equidistantly in the PETRA IV lattice. The results are shown in Fig. 15. After introducing one SC kick every 23 m, or 1/100th of the machine circumference, the final beam emittances converge to stable values and do not change with the addition of extra SC elements. In our numerical scans in ELEGANT, we used about 700 SC kicks, with the average distance between them being about 4 m.
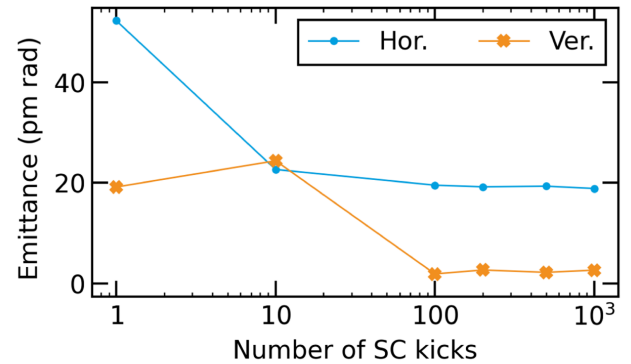

FIG. 15. Emittance after 10^4 turns of tracking with different amounts of equidistantly placed SC kicks. Bunch charge 10 nC, no transverse wakefields.
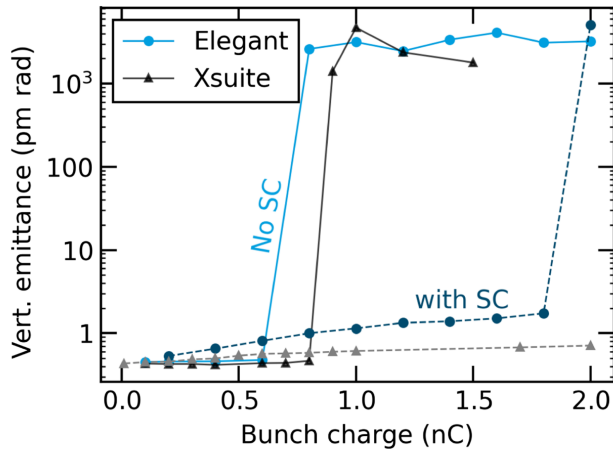
FIG. 16.   Charge scan comparison between ELEGANT (dots) and Xsuite (triangles). Only the main rf system is included, $\xi = 0$. Results without (solid curve) SC and with (dashed) SC kicks are shown.

APPENDIX B: BENCHMARKS WITH A PARTICLE-IN-CELL CODE Xsuite

In order to benchmark our quasifrozen SC model in ELEGANT, we performed a benchmark comparison with a particle-in-cell (PIC) model, implemented in Xsuite. The PIC SC kicks were introduced equidistantly along the lattice every 46 m (50 SC kicks in total). The typical setup for the PIC solver was (a) a transversal grid divided into 256×256 segments, range between ± 10 rms beam sizes; (b) 105 mm-long longitudinal grid with 100 divisions. Details on the implementation of the 2.5D PIC solver can be found in [27]. Particles were tracked for 10^4 turns, including the effects of synchrotron radiation, quantum excitation, and wakefields. The chromaticity was fully corrected, and only the main cavity was included. The results of this benchmark are illustrated in Fig. 16. The data shown in Fig. 5(c) are included as blue dots. The charge scan simulations are consistent with the results presented in Sec. III. Stabilization of TMCI is confirmed in both numerical models.

---

[1] W. T. Weng, Space charge effects—Tune shifts and resonances, AIP Conf. Proc. **153**, 348 (1987).

[2] H. Bartosik, F. Asvesta, A. Huschauer, Y. Papaphilippou, and F. Schmidt, Space charge induced losses in the CERN injector complex, J. Instrum. **15**, P07021 (2020).

[3] A. Oeftiger, O. Boine-Frankenheim, V. Chetvertkova, V. Kornilov, D. Rabusov, and S. Sorge, Simulation study of the space charge limit in heavy-ion synchrotrons, Phys. Rev. Accel. Beams **25**, 054402 (2022).

[4] M. Blaskiewicz, Fast head-tail instability with space charge, Phys. Rev. ST Accel. Beams **1**, 044201 (1998).

[5] V. Kornilov and O. Boine-Frankenheim, Head-tail instability and Landau damping in bunches with space charge, Phys. Rev. ST Accel. Beams **13**, 114201 (2010).

[6] V. Kornilov and O. Boine-Frankenheim, Space charge effects on Landau damping from octupoles, CERN Yellow Rep. Conf. Proc. **9**, 237 (2020).

[7] V. Balbekov, Transverse modes of a bunched beam with space charge dominated impedance, Phys. Rev. ST Accel. Beams **12**, 124402 (2009).

[8] A. Burov, Head-tail modes for strong space charge, Phys. Rev. ST Accel. Beams **12**, 044202 (2009).

[9] A. Burov, Head-tail modes for strong space charge, Phys. Rev. ST Accel. Beams **12**, 044202 (2009); **12**, 109901(E) (2009).

[10] A. Burov, Convective instabilities of bunched beams with space charge, Phys. Rev. Accel. Beams **22**, 034202 (2019).

[11] W. Decking and R. Brinkmann, Space charge problems in the TESLA damping ring, in *Proceedings of the 7th European Particle Accelerator Conference, EPAC-2000, Vienna, Austria* (EPS, Geneva, 2000), pp. 1024–1026.

[12] A. Xiao, M. Borland, L. Emery, Y. Wang, and K. Y. Ng, Direct space charge calculation in elegant and its application to the ILC damping ring, Conf. Proc. C **070625**, 3456 (2007).

[13] G. Rumolo, J. B. Jeanneret, Y. Papaphilippou, and D. Quatraro, Collective effects in the CLIC damping rings, Conf. Proc. C **0806233**, MOPP049 (2008).

[14] M. Zampetakis, F. Antoniou, F. Asvesta, H. Bartosik, and Y. Papaphilippou, Interplay of space charge, intrabeam scattering, and synchrotron radiation in the Compact Linear Collider damping rings, Phys. Rev. Accel. Beams **27**, 064403 (2024).

[15] D. Einfeld, M. Plesko, and J. Schaper, First multi-bend achromat lattice consideration, J. Synchrotron Radiat. **21**, 856 (2014).

[16] P. Raimondi *et al.*, The Extremely Brilliant Source storage ring of the European Synchrotron Radiation Facility, Commun. Phys. **6**, 82 (2023).

[17] R. Nagaoka and K. L. Bane, Collective effects in a diffraction-limited storage ring, J. Synchrotron Radiat. **21**, 937 (2014).

[18] G. Iadarola *et al.*, Xsuite: An integrated beam physics simulation framework, in *Proceedings of the 68th Advanced Beam Dynamics Workshop High-Intensity High-Brightness Hadron Beams (HB2023)* (JACoW, Geneva, Switzerland, 2024), pp. 73–80, 10.18429/JACoW-HB2023-TUA2I1.

[19] I. Agapov, S. Antipov, R. Bartolini, R. Brinkmann, Y.-C. Chae, E. C. Cortes-Garcia, D. Einfeld, T. Hellert, M. Huening, M. A. Jebramcik, J. Keil, C. Li, L. Malina, and R. Wanzenberg, Beam dynamics performance of the proposed PETRA IV storage ring, arXiv:2408.07995.

[20] A. Nadji and L. Nadolski, Upgrade project of the SOLEIL accelerator complex, Synchrotron Radiat. News **36**, 10 (2023).

[21] A. Loulergue, R. Nagaoka, O. Blanco-García, A. Gamelin, A. Nadji, M.-A. Tordeux, P. Brunelle, W. Foosang, and L. Nadolski, TDR baseline lattice for SOLEIL II upgrade project, in *Proceedings of the International Particle Accelerator Conference, IPAC-2023, Venice, Italy*

(JACoW, Geneva, Switzerland, 2023), Vol. 14, 10.18429/JACOW-IPAC2023-MOPM031.

[22] P. Alexandre, R. Ben El Fekih, F. Bouvet, and M.-A. Tordeux, Pulsed magnets and power supplies for injection & extraction in the SOLEIL II project, in *Proceedings of the 14th International Particle Acceletrator Conference, IPAC-2023, Venice, Italy* (JACoW, Geneva, Switzerland, 2023), pp. 4377–4380, 10.18429/JACoW-IPAC2023-THPA175.

[23] M. Bei, M. Borland, Y. Cai, P. Elleaume, R. Gerig, K. Harkay, L. Emery, A. Hutton, R. Hettel, R. Nagaoka, D. Robin, and C. Steier, The potential of an ultimate storage ring for future light sources, Nucl. Instrum. Methods Phys. Res., Sect. A **622**, 518 (2010).

[24] P. Raimondi, X. Huang, J. Kim, J. Safranek, and T. Rabedeau, Advanced storage ring lattice options based on hybrid six-bend achromat for Stanford Synchrotron Radiation Lightsource upgrade, Nucl. Instrum. Methods Phys. Res., Sect. A **1061**, 169137 (2024).

[25] K. Balewski, W. Brefeld, W. Decking, H. Franz, R. Rohlsberger, and E. Weckert, PETRA III: A low emittance synchrotron radiation source, DESY Technical Report No. DESY-04-035, 2004, 10.3204/PUBDB-2017-10776.

[26] J.-M. Filhol, J. C. Besson, P. Brunelle, M. E. Couprie, J. C. Denard, J. M. Godefroy, C. Herbeaux, P. Lebasque, V. Le Roux, M. P. Level, A. Lestrade, A. Loulergue, P. Marchand, J. L. Marlats, A. Nadji, L. Nadolski, R. Nagaoka, B. Pottin, and M.-A. Tordeax, Overview of the status of the SOLEIL project, in *Proceedings of the European Particle Accelerator Conference, EPAC-2006, Edinburgh, UK* (JACoW, Geneva, Switzerland, 2006), pp. 2723–2727, https://accelconf.web.cern.ch/e06/PAPERS/THXPA02.PDF.

[27] A. Oeftiger, Space charge effects and advanced modelling for CERN low energy machines, Ph.D. thesis, Ecole Polytechnique, Lausanne, LPAP, 2016, https://cds.cern.ch/record/2233212.

[28] I. Hofmann, *Space Charge Physics for Particle Accelerators, Particle Acceleration and Detection* (Springer, Berlin, 2017), 10.1007/978-3-319-62157-9.

[29] E. Métral, Imaginary tune split and repulsion single-bunch instability mechanism in the presence of a resistive transverse damper and its mitigation, Phys. Rev. Accel. Beams **24**, 041003 (2021).

[30] S. Liuzzo *et al.*, Optimisation of the ouschek lifetime in synchrotron light sources using adger, in *Proceedings of the 19th International Conference on Accelerator and Large Experimental Physics Control Systems, ICA-LEPCS2023, Cape Town, South Africa* (JACoW, Geneva, Switzerland, 2023), MO3AO01, 10.18429/JACoW-ICA-LEPCS2023-MO3AO01.

[31] B. Zotter, Single-bunch instabilities in circular accelerators, in *Handbook of Accelerator Physics and Engineering*, 2nd ed., edited by A. W. Chao, K. H. Mess, M. Tigner, and F. Zimmermann (World Scientific, Singapore, 2013), p. 149.

[32] A. Macridin, A. Burov, E. Stern, J. Amundson, and P. Spentzouris, Simulation of transverse modes with their intrinsic Landau damping for bunched beams in the presence of space charge, Phys. Rev. ST Accel. Beams **18**, 074401 (2015).

[33] M. Borland, Elegant: A flexible SDDS-compliant code for accelerator simulation, in *Proceedings of the 6th International Computational Accelerator Physics Conference (ICAP 2000)* (2000), 10.2172/761286.

[34] R. Bartolini, Touschek and intrabeam scattering in ultralow emittance storage rings, in *Proceedings of the 13th International Particle Accelerator Conference, IPAC2022, Bangkok, Thailand* (JACoW, Geneva, Switzerland, 2022), MOIYSP2, 10.18429/JACoW-IPAC2022-MOIYSP2.

[35] M. Bassetti and G. A. Erskine, Closed expression for the electrical field of a 2D Gaussian charge, CERN, Geneva, Switzerland, Technical Report No. CERN-ISR-TH/80-06, 1980, https://cds.cern.ch/record/122227.

[36] G. Loisch (private communication).

[37] A. Gamelin, W. Foosang, N. Yamamoto, V. Gubaidulin, and R. Nagaoka, mbtrack2 (2024) (version 0.7.0), 10.5281/zenodo.12749990.

[38] A. Gamelin, W. Foosang, and R. Nagaoka, MBTRACK2, a collective effect library in Python, in *Proceedings of the 12th International Particle Accelerator Conference, IPAC-2021, Campinas, SP, Brazil* (JACoW, Geneva, Switzerland, 2021), 10.18429/JACoW-IPAC2021-MO-PAB070.

[39] N. Mounet, Landau damping in the transverse plane, CERN Yellow Rep. Conf. Proc. **9** 45 (2020).

[40] V. Kornilov, A. Oeftiger, O. Boine-Frankenheim, V. Chetvertkova, S. Sorge, and P. Spiller, Beam quality and beam loss predictions with space charge for SIS100, J. Instrum. **15**, P07020 (2020).

[41] V. Gubaidulin, A. Gamelin, A. Loulergue, R. Nagaoka, and P. Schreiber, Transverse instabilities in SOLEIL II storage ring in the presence of a harmonic cavity, in *Proceedings of the 15th International Particle Accelerator Conference, IPAC-2024, Nashville, TN* (JACoW, Geneva, Switzerland, 2024), 10.18429/JACoW-IPAC2024-MOPS45.

[42] R. Bruce, J. M. Jowett, M. Blaskiewicz, and W. Fischer, Time evolution of the luminosity of colliding heavy-ion beams in BNL Relativistic Heavy Ion Collider and CERN Large Hadron Collider, Phys. Rev. ST Accel. Beams **13**, 091001 (2010).

[43] K. Kubo, S. K. Mtingwa, and A. Wolski, Intrabeam scattering formulas for high energy beams, Phys. Rev. ST Accel. Beams **8**, 081001 (2005).

[44] G. Skripka, R. Nagaoka, M. Klein, F. Cullinan, and P. F. Tavares, Simultaneous computation of intrabunch and interbunch collective beam motions in storage rings, Nucl. Instrum. Methods Phys. Res., Sect. A **806**, 221 (2016).

[45] F. Cullinan, R. Nagaoka, G. Skripka, and P. Tavares, Transverse coupled-bunch instability thresholds in the presence of a harmonic-cavity-flattened rf potential, Phys. Rev. Accel. Beams **19**, 124401 (2016).